



## Late Holocene (~2 ka) East Asian Monsoon variations inferred from river discharge and climate interrelationships in the Pearl River Estuary



Qingyun Nan<sup>a,\*</sup>, Tiegang Li<sup>a</sup>, Jinxia Chen<sup>b</sup>, Rajiv Nigma<sup>c</sup>, Xinke Yu<sup>a</sup>, Zhaokai Xu<sup>a</sup>, Zaibao Yang<sup>a</sup>

<sup>a</sup> Key Laboratory of Marine Geology and Environment, Institute of Oceanology, Chinese Academy of Sciences, Qingdao 266071, China

<sup>b</sup> First Institute of Oceanology, State Oceanic Administration, Qingdao 266071, China

<sup>c</sup> National Institute of Oceanography, Dona Paula, Goa 403004, India

### ARTICLE INFO

#### Article history:

Received 12 March 2013

Available online 15 January 2014

#### Keywords:

East Asian Monsoon

Late Holocene

River discharge

ENSO

Pearl River Delta

### ABSTRACT

A sediment core from the Pearl River Estuary (PRE) was analyzed for grain size and organic geochemistry parameters (TOC and  $\delta^{13}\text{C}_{\text{org}}$ ). The results showed that high mean grain-size value and increased sand content were correlated with the high TOC and negative  $\delta^{13}\text{C}_{\text{org}}$ . These results indicated high river runoff in the PRE area. Peak river discharge occurred during the periods 1900–1750, 1500–1600, 1400–1200, 1000–900 and 750–600 cal yr BP. The main changes recorded in grain-size distributions, TOC contents, and  $\delta^{13}\text{C}_{\text{org}}$  variations appear to be directly related to monsoon precipitation in the sediment source area. An increased East Asian summer monsoon rainfall (EASM) and/or an enhanced East Asian winter monsoon rainfall could result in the increasing of monsoon rainfall. Typhoon related rainfalls could act as positive influence on precipitation levels. The study of the correlations between the rainfall records and ENSO activities revealed a close relationship between the monsoon rainfall in the PRE and the tropical Pacific variations. The frequent occurrence of ENSO might result in the southern migration of the EASM rain belt and lead to more typhoon-derived rainfall in the PRD during the late Holocene.

© 2013 University of Washington. Published by Elsevier Inc. All rights reserved.

### Introduction

The relationship between historical cultural evolution and environmental changes has aroused considerable interest over recent years (Jousse and Escarguel, 2006; Iriondo et al., 2009; Sasaki and Takahara, 2011). Records show that the collapse of some civilizations has been close in time to abrupt climatic changes (Cullen et al., 2000; de Menocal, 2001; Wahl et al., 2006). In China, archeological data show that dynastic changes have corresponded with changes in climate (Wu and Liu, 2004; Hollmes et al., 2009). Although new proxy data have now been obtained, an integrated view of natural climate variability and its influences on the development/collapse of cultural evolution during the late Holocene is yet to be realized. Solutions to this problem will require high-quality, high-resolution proxy records gathered from even more climatically sensitive and regionally representative locations.

Estuarine deltas on continental shelves provide ideal sites for studying climate records on decadal to centennial time scales. The formation of a salinity front induces the deposition of terrigenous materials, resulting in a relatively high sedimentation rate (Zhou et al., 2012a). Furthermore, through water mass exchanges, sediments in the estuarine delta area contain paleoenvironmental information of the hinterland as

well as paleoceanographic variability on the adjacent continental margins and shelves (Tanabe et al., 2006; Smith et al., 2011). Therefore, sediments in estuarine deltas offer an excellent opportunity to study land–ocean interactions.

The Pearl River Estuary (PRE) is located on the continental shelf of South China Sea (SCS). It is well-suited for studying paleoenvironmental patterns (Zong et al., 2006). The PRE is a typical weak tide estuary. Water mass exchanges in the estuary are mainly controlled by the intrusion intensity of riverine freshwater (Wong et al., 2004). This makes the sedimentation quite sensitive to local hydrological changes. Furthermore, the PRE and the Pearl River catchment are both located in an area which is influenced by the East Asian Monsoon (EAM) (Jilan, 2004). Long-term variations in monsoon intensity result in fluctuations in the amount of precipitation and, hence, freshwater flux through major estuarine systems into the sea (Zong et al., 2006). Furthermore, the warm climate and abundant precipitation in this area cause a large amount of terrestrial input into the PRE. This leads to high sedimentation rates (Chen et al., 1993) and improves the opportunity for a high-resolution investigation. Additionally, records from the PRE may provide useful information about the connection between the EAM evolution and variations in the tropical Pacific warm pool because the heat and moisture found in the tropical Pacific have a close relationship with the EAM system (Wang et al., 1997). Furthermore, it is believed that a persistent El Niño stage causes a strengthened monsoon rainfall in southern China (Wang et al., 2000b; Wu et al., 2003; Zeng et al., 2011). Modern observation shows that annual rainfall differs dramatically

\* Corresponding author at: Key Laboratory of Marine Geology and Environment, Institute of Oceanology, Chinese Academy of Sciences, 7 Nanhai Road, Qingdao 266071, China.

E-mail address: [nanqingyun@qdio.ac.cn](mailto:nanqingyun@qdio.ac.cn) (Q. Nan).

between the monsoon-enhanced wet years and the monsoon-reduced dry years (as the ratio of the maximum to minimum annual rainfall and river runoff is about 2–3 times and 4–6 times, respectively, in the PRE) (Jilan, 2004). Strong positive correlations between sediment load and freshwater discharge in the PRE suggest that sediment is highly sensitive to rainfall caused by monsoon intensity (Zhang et al., 2012). Therefore paleoenvironmental proxies reconstructed from this estuarine sediment can be used to trace the history of EAM variability (Zong et al., 2006, 2009; Yu et al., 2012; Zong et al., 2012).

A great deal of research has been carried out in the PRE area since the 1980s. This data has been synthesized by Huang et al. (1982) and Li (1991). Most of this research focused on the formation history of the Pearl River Delta (Li, 1991, and references therein); the relative sea-level variations (Li, 1985; Zong, 2004; Zong et al., 2009, 2012); local coastline migration (Long and Huo, 1990; Huang et al., 2004; Li, 2004; Zong et al., 2010a), and vegetation history and its response to climate change (Shen et al., 1989; Wang et al., 2007a) since the last glacial period. Few records have focused on the paleoenvironmental changes in the Holocene (Huang et al., 1997; Zhang and Huang, 2005; Zong et al., 2006; Dong et al., 2007; Zong et al., 2009; Yu et al., 2010; Zong et al., 2010a,b,c) in the PRE.

Though the relative sea level (RSL) changed dramatically in the early Holocene, available data show a stable sea level over the past several thousand years (Zong, 2004; Cheng and Qi, 2007), hence changes in RSL will have minimal impact on the PRE. Previous studies in the Pearl River Estuary have shown that changes in the  $\delta^{13}\text{C}_{\text{org}}$  and C/N ratios of estuarine sediments can be used as an indicator for changes in the freshwater discharge induced by the monsoonal precipitation for the mid to late Holocene (Zong et al., 2006; Yu et al., 2012; Zong et al., 2012). Zong et al. (2006) first employed bulk organic carbon isotope ( $\delta^{13}\text{C}_{\text{org}}$ ) and total carbon/nitrogen (C/N) ratios to reconstruct the Holocene monsoon history in the PRE. Yu et al. (2010) and Zong et al. (2010b) employed the similar proxies and discussed the Holocene monsoon rainfall and material delivery history in the PRE. Yu et al. (2012) revealed high-resolution (~20 yr) mid-Holocene variability of the East Asian monsoon history and Zong et al. (2012) provided evidence of human activity for the last 4000 cal yr BP in the PRE. However, rarer studies have focused on the most recent 2000 yr due to the limitation of high-resolution climatic records in the PRE.

In this study, we present a high-resolution (average: ~7 yr), late Holocene record for the central PRE. This research is based on grain-size distribution, total organic carbon (TOC) contents, and  $\delta^{13}\text{C}_{\text{org}}$ . We hope to be able to provide a detailed late Holocene history of the East Asian monsoon climate. In this way, we will attempt to explore the possible causes that are responsible for changes in monsoonal precipitation over the PRE.

## Regional settings

The Pearl River (PR, also named as Zhujiang River) is the second largest river in China and the 13th largest river in the world in terms of discharge volume. It is formed primarily by the confluence of three principal rivers: the West River, the North River and the East River (Fig. 1). The Pearl River delivers  $350 \times 10^9 \text{ m}^3/\text{yr}$  of fresh water with a sediment load of  $85 \times 10^6 \text{ t}/\text{yr}$  into the South China Sea. This volume is delivered via three estuaries, Lingdingyang, Modaomen, and Huangmaohai (Fig. 1). The Lingdingyang (named the Pearl River Estuary (PRE) in this study) receives over 50% of the Pearl River freshwater discharge (Jilan, 2004) and is the primary focus of this study.

The PRE is a dynamic and complex estuary with four river inlets. They are named: Humen (HUM), Jiaomen (JIM), Hongqili (HQL) and Hengmen (HEM) (Fig. 1). Except for the deep channels and the areas around the outer islands where the water depth varies between 20 and 30 m, most of the PRE is quite shallow. It has an average water depth between 2 and 10 m. The PRE is located along a micro-tidal coast with an average tidal range of about 1 m. The combined effect of

a small tidal range and large bay area results in the PRE being a good place for sediment deposit (Jilan, 2004).

The Pearl River catchment covers a region of subtropical to tropical maritime monsoon climate. The monthly air temperature and precipitation range from ~6°C to 34°C and 45 mm to 280 mm at Guangzhou (the area adjacent to the PRE: Fig. 2). The monsoon is the dominant climatic controlling factor in the Pearl River Delta (PRD). In the summer wet seasons (April–September) when the southwest monsoon prevails, about 98.68% of the sediment load, and 77.80% of the water are delivered into the PRE (Jilan, 2004). Meanwhile, in the dry winter seasons (from October to March) when the northeast monsoon prevails, only 1.3% of the sediment load and 22.2% of the water are delivered (Zhang et al., 2012). In addition, the impact of tropical cyclones on this region is more concentrated during 7–9 months of the year. When tropical cyclones make landfall near the PRD, extreme rainfall occurs in the drainage areas (Liu et al., 2001). Therefore, the combination of tropical cyclones and monsoon rainfall provides the peak precipitation in the PRD.

Water regimes in the PRE are basically controlled by the interaction of riverine freshwater and salt shelf water (Chen et al., 2004). During the wet season, less-dense freshwater dominates the surface of PRE and the front extends across the estuary (Dong et al., 2004). Here, the salinity varies from 1 to ~20 (Wong et al., 2004) (Fig. 3a). The salty oceanic water intrudes along the axis of the estuary. The bottom salinity increases across the estuary from the west to east (Fig. 3b). A strong density and salinity gradient is found in the PRE during the wet season. This gradient benefits for the deposition of the river-load material (Gao and Michael, 2001). In the dry season, due to the substantially reduced river runoff, the high salinity shelf water intrudes into the PRE and mixes with the riverine water. Here, the water in the PRE is partially stratified compared to the wet seasons (Figs. 3c, d). In sharp contrast to the great difference of salinity, there is only a small difference (<2°C) between the surface and bottom water temperatures (Zhou et al., 2011).

During the rainy season, heavy rains bring a large amount of freshwater into the PRE. This influx pushes the denser seawater towards the open shelf. A turbidity layer in the upper PRE is generated and it moves towards the central and southeast parts of the PRE. This results in a northwest to southeast decrease in the median grain size (MZ) distribution and the content of coarser sediment components (Peng et al., 2004).

In the PRE, the organic materials are composed of terrestrial organic matter and plankton-derived organic matter. The balance between terrestrial organic matter and in situ plankton-derived organic matter is strongly influenced by the strength of the freshwater runoff (Fig. 3e) (Yu et al., 2010). During the wet summer, heavy monsoonal precipitation results in a remarkable increase in terrestrial organic matter input into the PRE. Meanwhile, during the dry winter, the significant reduction in monsoonal precipitation results in a remarkable reduction in the terrestrial organic matter. At this time, the organic matter within the estuary is dominated by in situ phytoplankton. Since most of the sediment load in the PRE is delivered during the wet season (Zhang et al., 2012), a clear trend of terrestrial organic matter contribution (TOM%) is high in the three main river inlet areas (up to 90%) HQL, HEM, JTM (Fig. 3e). Meanwhile less than 20% is found in the southeast of the PRE. This is because it is quite far away from the freshwater-influenced area (Yu et al., 2010).

## Materials and methods

In order to obtain the undisturbed sediment sequences we collected a gravity core Z09-Z (113.7784°E, 22.3501°N, water depth at the coring site is 8.4 m) on the subtidal flat at the edge of the central shallow of the Pearl River Estuary (Fig. 1). This pro-delta area is away from the two main tidal channels (Zong et al., 2010b). Moreover, the core site locates

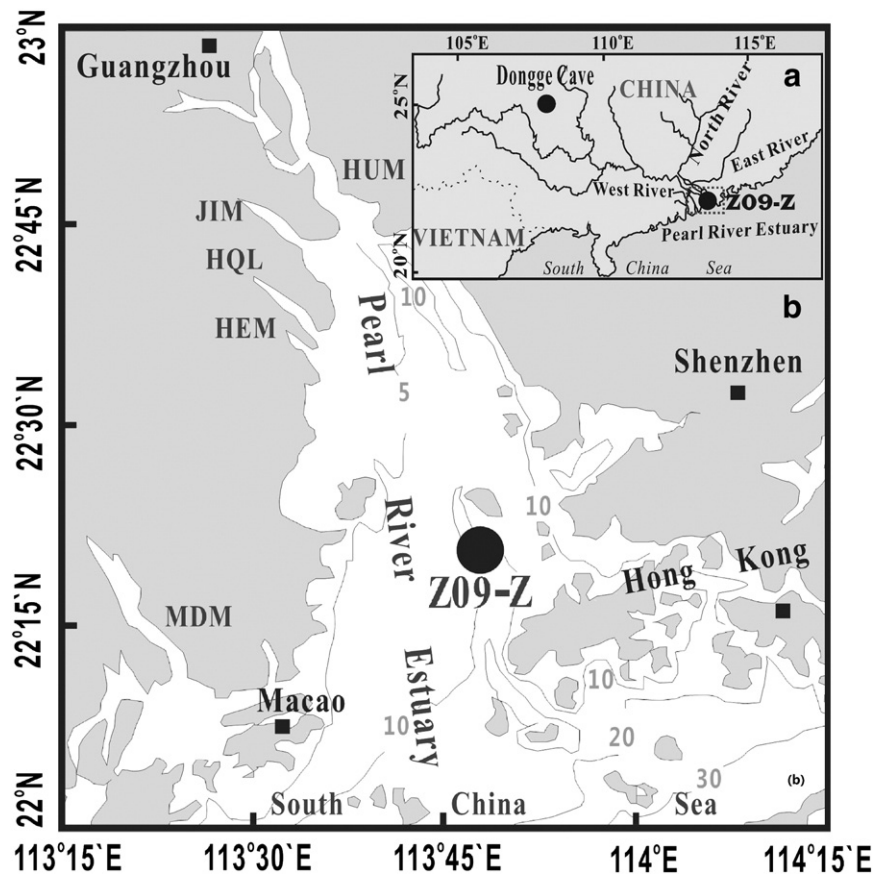


**Figure 1.** Location of the study area located within the Pearl River Delta and Estuary. The drainage system, and sample site are shown within the estuary (sea floor topography data is based on Wong et al., 2004). The position of the Dongge Cave stalagmite D4 is also shown. Five main river inlets (Humen, Jiaomen, Hongqili, Hengmen and Modaomen) are labeled in acronyms as HUM, JIM, HQL, HEM and MDM, respectively.

between the Nei Lingding Island and Lantau Island and is protected from strong typhoon storms (Fig. 1).

The core was obtained using a 110 mm (in diameter) gravity sampler with a plastic tube inside the corer to capture and protect the sediment samples from disturbance. The topmost part of the sediment (~30 cm in depth) was lost when the plastic tube was pulled out from the gravity sampler due to very high water content. The recovered core can be lithologically divided into four units from top to base. Between 0 cm and 45 cm, the sediment consists of undisturbed very soft dark gray clay. The depth from 45 to 130 cm is mainly composed of dark-gray clay with several imbedded dark clay layers and the

interval from 180 to 130 cm is composed of dark-gray silty clay. The depth from 284 to 180 cm is mainly composed of gray silty clay with slim imbedded sand layers (Fig. 4). From a visual inspection there were no considerable disturbances in the entire core.

Once the tubes were opened in the laboratory, the sediment cores were split, described in detail, and sampled at 1-cm intervals. The sub-samples were analyzed for particle size, TOC and  $\delta^{13}\text{C}_{\text{org}}$ .

For the grain-size analysis, samples were pretreated with 10–20 ml of 30%  $\text{H}_2\text{O}_2$  for 4 h to remove organic matter. This was followed by an acidification process to remove carbonate with 4 ml 7% HCl for 24 h. Then, the non-carbonate samples were rinsed with deionized water 4 times to

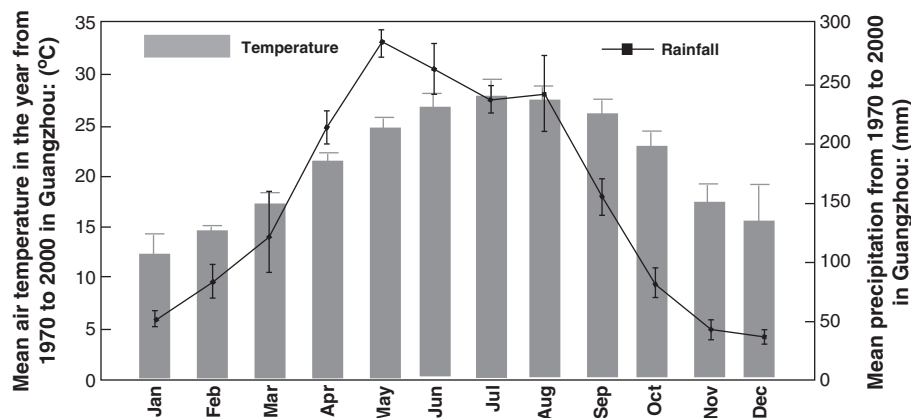


**Figure 2.** Annual changes in monthly mean air temperature and mean precipitation. These are the average figures from the Guangzhou meteorological monitoring station (1970–2009). The data have been adapted from Kuang et al. (2008) and Chen et al. (2012).

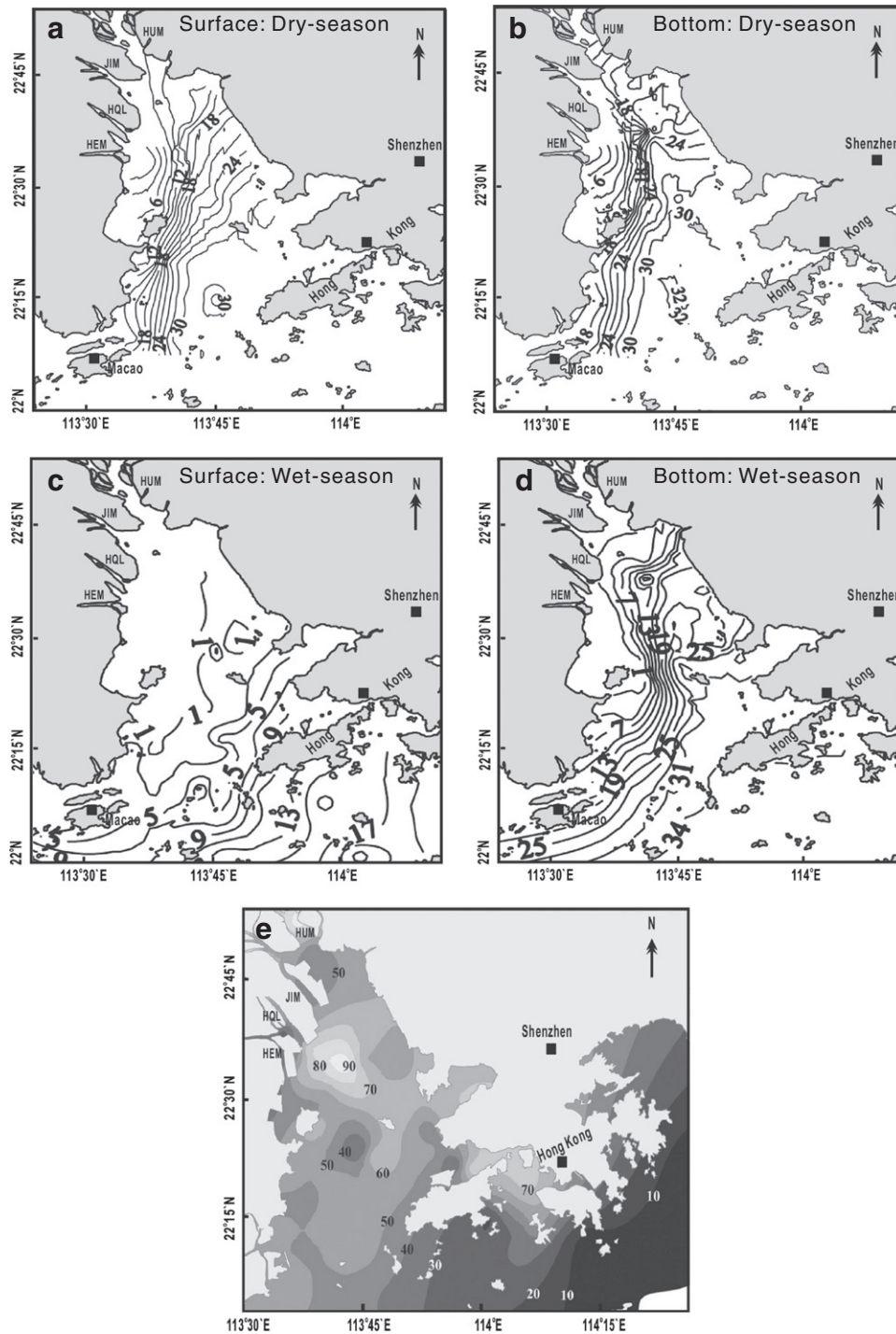


**Figure 3.** Contour maps showing mean seasonal salinity (a, b, c, d) in adjacent coastal waters (modified from Harrison et al., 2008), as well as the terrigenous organic contribution to the surface sediment (e) within the Pearl River Estuary (Yu et al., 2010). Surface water salinity in the dry season (a), bottom water salinity in the dry season (b), surface water salinity in the wet season (c), bottom water salinity in the wet season (d), and the distribution of terrigenous organic matter (TOM%) to the surface sediment (e).

remove residual acid and salt. An ultrasonic process was then used to facilitate dispersion before the grain-size analysis. Grain-sizes were analyzed with a Cilas 940 l instrument in the Key Laboratory at the Marine Geology and Environment Science, Chinese Academy of Sciences.

For the geochemical analyses of organic carbon content and isotopes, the freeze-dried and homogenized samples were acidified for 48 h with 1 mol/l HCl. They were then rinsed four times with deionized water to remove carbonate carbon. Then, the samples were freeze-dried, ground, and homogenized with an agate mortar. The TOC content in the carbonate-free samples was determined using a Thermal EA 1112

CHN elemental analyzer. The combustion temperature was 960°C. The results were then reported as gram TOC or TN per hundred-gram whole sediment (%). The relative precision for the experimental procedure was estimated to be 0.1% based on the repeated measurements of a standard. Samples for  $\delta^{13}\text{C}$  analysis were weighed into clean tin capsules and placed in an elemental analyzer. They were then burned at 1050°C in a pure  $\text{O}_2$  atmosphere within a combustion tube. The combustion gases were swept through a reduction column by a stream of He gas and separated into  $\text{CO}_2$  and  $\text{N}_2$  by a gas chromatography. Then, the gas stream entered a GV-Isoprime mass spectrometer where the  $\text{CO}_2$

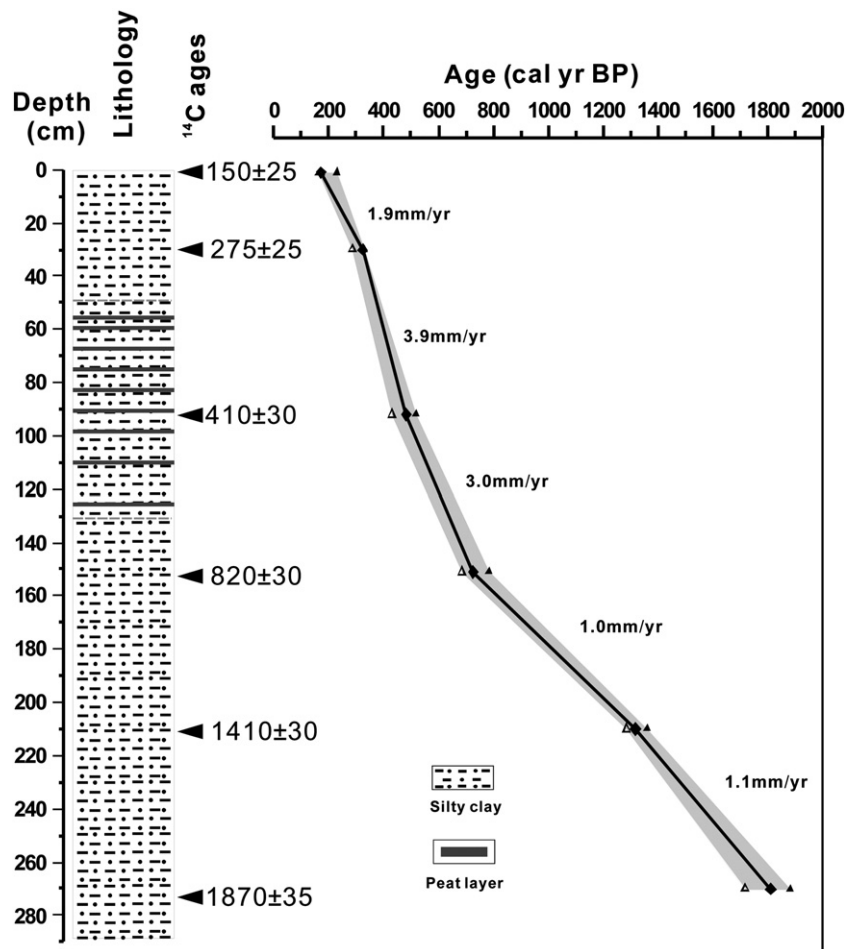


**Figure 4.** Lithology and age–depth model for core Z09-Z. The age-model is based on a linear interpolation of the calibrated AMS<sup>14</sup>C dates. These figures were obtained by using Calib 6.0 software (by Stuiver, <http://calib.qub.ac.uk/calib/>). The open triangle, diamond and solid triangle represent the start, median and end calibration ages with 2- $\sigma$  precision. The gray envelope shows the 2- $\sigma$  precision age ranges. The linear sediment accumulation rates are listed beside the time–depth curve.

was analyzed and compared to the internal gas standard. Sample isotope ratios were compared to pure cylinder CO<sub>2</sub> injected directly into the mass spectrometer before the sample peaks and provisional  $\delta^{13}\text{C}$  (PDB) values were calculated. The provisional isotope values were adjusted in order to bring the mean values of working standard samples distributed at intervals in each analytical run to the correct values of the working standards. The working standard was Urea with  $\delta^{13}\text{C}$  vs. PDB =  $-27.00\%$ . The standard was periodically calibrated against international isotope standards (IAEA N1). The average precision

calculated by a replicated analysis of the internal standard was 0.12‰ for  $\delta^{13}\text{C}$ .

A total of six AMS<sup>14</sup>C dates were obtained for the Z09-Z core. Due to the lack of carbonate detritus, all AMS<sup>14</sup>C dating was based on hand-picked terrestrial plant charcoal fragments. Four AMS<sup>14</sup>C dates were measured at the National Ocean Sciences AMS testing central (WHOI). Another two AMS<sup>14</sup>C dates were measured in the Accelerator Mass Spectrometry Laboratory, Peking University (Table 1). The original AMS<sup>14</sup>C dates derived from the terrestrial organic matter were then

**Table 1**  
AMS radiocarbon age data for PRE core Z09-Z.

Depth (cm)	Dating material	AMS <sup>14</sup> C age ( <sup>14</sup> C yr BP)	1 $\sigma$ -calibrated range (yr BP)	2 $\sigma$ -calibrated range (yr BP)	Median calibrated <sup>14</sup> C age (cal yr BP) <sup>a</sup>
0–1 <sup>b</sup>	Charcoal/plant fiber	150 ± 25	172–223	168–231	173 ± 50
29–31 <sup>b</sup>	Charcoal/plant fiber	275 ± 25	293–317	285–330	324 ± 50
90–94 <sup>c</sup>	Charcoal/plant fiber	410 ± 30	464–509	429–519	483 ± 60
150–152 <sup>b</sup>	Charcoal/plant fiber	820 ± 30	690–742	684–783	727 ± 60
208–212 <sup>c</sup>	Charcoal/plant fiber	1410 ± 30	1296–1332	1285–1359	1317 ± 60
268–272 <sup>b</sup>	Charcoal/plant fiber	1870 ± 35	1807–1868	1717–1881	1811 ± 70

<sup>a</sup> The original AMS<sup>14</sup>C dates have been converted to calibrated ages before 1950 AD (cal yr BP) using the Calib 6.0 (by Stuiver, <http://calib.qub.ac.uk/calib/>) and the IntCal09 calibration datasets (Reimer et al., 2009). The 1- $\sigma$  and 2- $\sigma$  age ranges are listed within the table. The median calibrated ages were used for calculating the linear sedimentary ratio.

<sup>b</sup> AMS<sup>14</sup>C dating was done in the National Ocean Sciences AMS testing central (WHOI).

<sup>c</sup> AMS<sup>14</sup>C dating was done in the Accelerator Mass Spectrometry Laboratory, Peking University.

converted to calibrated ages before 1950 AD (cal yrs BP) using the Calib 6.0 (by Stuiver, <http://calib.qub.ac.uk/calib>) and the IntCal09 calibration datasets (Reimer et al., 2009). An age–depth model was developed using linear interpolation between calendar ages.

## Results

### Radiocarbon chronology

The core Z09-Z has a calibrated age ranging from ca. 1910 cal yr BP to ca. 173 cal yr BP (Fig. 4). The estimated surface age of around 173 cal yr BP indicates that sediments younger than 170 yr BP were probably removed during core sampling. Even though this age model indicates that the studied core covers a time interval of about 1750 yr during the late Holocene, accumulation rates through the core are relatively high. The average accumulation rates were calculated to be 1.9 mm/yr, 3.9 mm/yr, 3.0 mm/yr, 1.0 mm/yr, and 1.1 mm/yr for time intervals of 173–324 cal yr BP, 324–483 cal yr BP, 483–727 cal yr BP, 727–1317 cal yr BP and 1317–1910 cal yr BP, respectively. Our records are therefore consistent with the conclusions of Yao et al. (2008), whose research suggests an average sedimentation of 2.0 mm/yr within the PRE area.

### Grain-size distribution

Data for grain-size distribution (Ms,  $\mu\text{m}$ ; clay, %; silt, %; sand, %) in the Z09-Z core sediments spanning the last ca 2000 yr were plotted against calibrated radiocarbon ages. Figures 5a–c and d show the vertical variation of the percentages of clay (<4  $\mu\text{m}$ ), silt (4–63  $\mu\text{m}$ ) and sand (>63  $\mu\text{m}$ ) contents, as well as the mean grain-size distribution. The core sediment consisted of 20–50% clay, 40–70% silt, 0–10% sand, and was poorly sorted (1.3–1.9  $\phi$ ). For the late Holocene, the variation in the proportion of clay and silt suggested a two-stage evolution. Before 600 cal yr BP, the silt and clay fraction content showed clear fluctuations. There were high silt percentage (low clay percentage) episodes at ca. 1900 cal yr BP, 1800 cal yr BP, 1600 cal yr BP, 1450 cal yr BP, 1350 cal yr BP, 1000 cal yr BP, and 720 cal yr BP. After 600 cal yr BP, the silt content remained relatively stable and showed a gradually trend towards reduction.

Compared with the high content of clay and silt, the sand content is negligible for much of the late Holocene in the Z09-Z core. This is due to its extremely low percentage (<1%). However, peak sand values were recorded at about 1900 cal yr BP, 1800 cal yr BP, 1600 cal yr BP, 1350 cal yr BP, 1000 cal yr BP, 950 cal yr BP, and 720 cal yr BP. This corresponds quite well with the high silt percentages. The MZ shows similar variations with the silt content, with high values corresponding to sand peak values. This suggests a relatively high portion of coarse fraction.

### TOC and $\delta^{13}\text{C}_{\text{org}}$

Total organic carbon concentrations generally remained between 0.6% and 1.2% throughout the sediment record over the last 2000 cal yr BP. It reached a sharp maximum of 1.44% at ca. 900 cal yr BP (Fig. 5e). A two stage variation was revealed by the TOC percentages, with an increasing trend from ca. 1900 cal yr BP to 900 cal yr BP, and a high-frequency oscillation period after 600 cal yr BP.

The bulk organic carbon isotopic compositions ranged between  $-21.1\text{‰}$  and  $-25.3\text{‰}$  (Fig. 5f). Here, there was an average of  $-22.6\text{‰}$  and  $-23.4\text{‰}$  before and after 1000 cal yr BP, respectively. Unlike the increasing trend of TOC, the  $\delta^{13}\text{C}_{\text{org}}$  values demonstrated large shifts in the range of  $-21.0$  and  $-24.6\text{‰}$  before 900 cal yr BP. There were also relatively negative shifts at 1850 cal yr BP, 1750 cal yr BP, 1600 cal yr BP, 1350 cal yr BP, 1100 cal yr BP, 950 cal yr BP and 720 cal yr BP. These similar high-frequency oscillations recorded in the  $\delta^{13}\text{C}_{\text{org}}$  after 600 cal yr BP, with negative values, correlated with

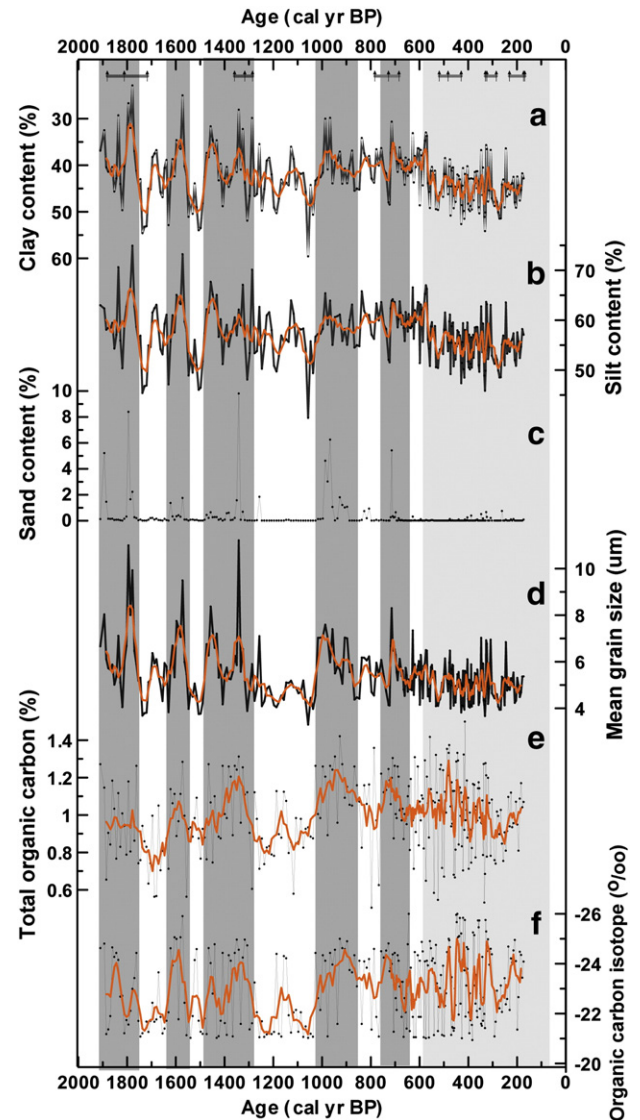


**Figure 5.** Grain-size distribution, total organic carbon content and bulk organic carbon isotopic values of core Z09-Z. (a) Component percentages of clay (<4  $\mu\text{m}$ ), (b) component percentages of silt (4–63  $\mu\text{m}$ ), (c) component percentages of sand (>63  $\mu\text{m}$ ), (d) the mean grain-size profile of the core Z09-Z, (e) total organic carbon content (TOC) and (f) bulk organic carbon isotopic composition. The 5-point moving average lines are highlighted in bright color lines. The black arrows in the top of the figure represent the calibrated 2- $\sigma$  start, median and end ages of each dating point. The slim shaded bars indicate the 2- $\sigma$  age ranges. The vertical thicker shaded sections represent the five peak river discharge periods recorded in core Z09-Z and the light gray vertical section represents the period of increasing human activities.

the high TOC contents, might correspond to the imbedded dark clay layers (Figs. 4, 5e, f).

## Discussion

### River discharge and a regional precipitation history of the PRE

Recent research has shown that the sediment load in the PRE has a strong association with water discharge (Yu et al., 2010; Zong et al., 2010a, 2010b, 2010c; Yu et al., 2012). This is characterized by the coincidence of high sediment load and high water discharge during the wet season (Zhang et al., 2012). Sediment transport reaches its peak during periods with the same level as the water discharge. For river basins, sediment yield is generally controlled by the magnitude and frequency of rainfall events (Zong et al., 2006). Therefore, it is likely to be sensitive to regional precipitation (Wang et al., 2007b).

Grain-size distribution curves of natural sediments have long been used to identify the type of depositional environments (Gao and Michael, 2001; Yu et al., 2012). Particle-size analysis is generally used to reveal the depositional environment (Owen, 2005; Fan et al., 2006; Huang et al., 2011), as well as hydrodynamic conditions (Sun et al., 2003) in the sediment cores. In continental shelf and lacustrine sediments, the variations in grain-size character (such as MZ, clay, silt and sand content) can be linked with changes to local rainfall and/or river runoff (Xu, 2000; Gao and Michael, 2001; Owen, 2005). In estuary regions where river flow has a great influence on the sediment, an

abrupt increase of mean grain size is inferred to have been transported by a sudden strengthening of river discharge (Xiao et al., 2006; Holz et al., 2007; Dinakaran and Krishnayya, 2011). More recently, grain-size characteristics have served as a proxy for the reconstruction of variations in East Asian monsoons in the Bohai Sea (Yi et al., 2012), the Yellow Sea (Zhou et al., 2012b), the East China Sea (Qiao et al., 2011), and the South China Sea (Huang et al., 2011). As illustrated in this research, increasing mean size values and higher sand content have suggested a higher fluvial contribution derived from the enhanced monsoon rainfall.

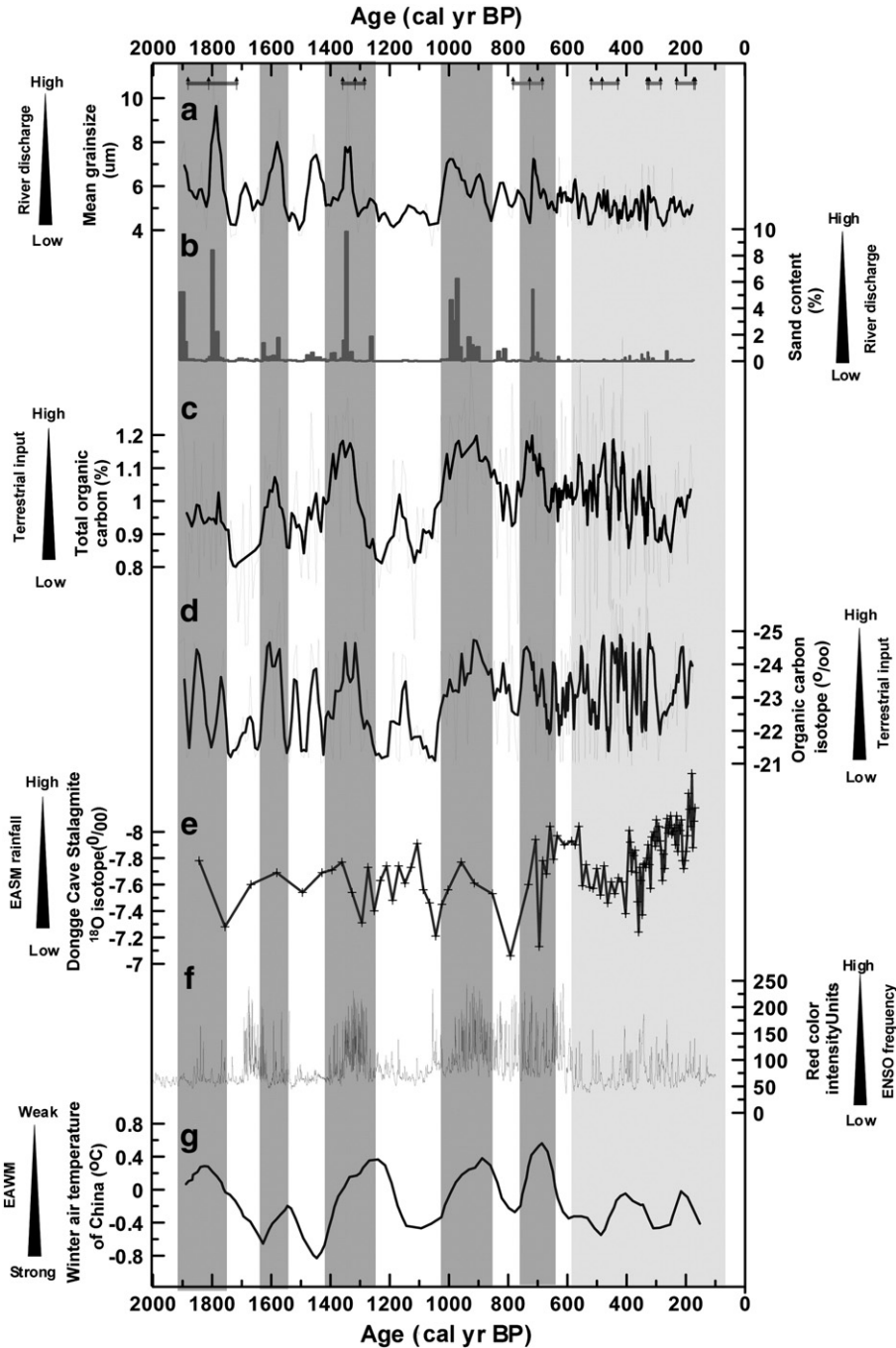


**Figure 6.** A comparison of Z09-Z records from PRE, to several late Holocene records from 2000 cal yr BP to present (1950). (a) 5-step running averages of the MZ; (b) sand content distribution; (c) 5-step running averages of the TOC content; (d) 5-step running averages of the  $\delta^{13}\text{C}$  values; (e) the stalagmite  $\delta^{18}\text{O}$  records from Dongge Cave (Dykoski et al., 2005) (East Asian Summer Monsoon rainfall); (f) the red color intensity unit records from Laguna Pallacocha, southern Ecuador (Moy et al., 2002) (ENSO frequency); (g) 2000-yr Chinese winter air temperature records (Wang and Wang, 1990; Zheng and Zheng, 1993; Guo et al., 2002) (East Asian Winter Monsoon). The black arrows in the top of the figure represent the calibrated 2- $\sigma$  start, median and end ages of each dating point. The slim shaded bars indicate the 2- $\sigma$  age ranges. The vertical thicker shaded sections represent the five peak river discharge periods recorded in core Z09-Z and the light gray vertical section represents the period of increasing human activity.

In general, high precipitation rates would enhance the soil erosion over the Pearl River Delta region (Zhang and Lu, 2009; Zong et al., 2010b). This would also increase the transport capacity of rivers and lead to more coarser clastic materials being available for river transport and subsequent deposition in the PRE (Li, 1991; Yu et al., 2012). Research from Huang and Yan (1997) and Peng et al. (2004) reveals that sediment grain size significantly coarsens during strong monsoon rainfalls and periods influenced by typhoons.

As shown in Figures 6a and b, the 5-step running averages of the MZ and sand-content values were relatively high during the periods 1900–1750 cal yr BP, 1500–1600 cal yr BP, 1400–1200 cal yr BP, 1000–900 cal yr BP, and around 700 cal yr BP. This would suggest an increase in freshwater discharge in the PR and hence increased precipitation over the PRE drainage area.

Organic matter constitutes a minor fraction of terrestrial and marine sediments, but it is an important part of their paleoclimatic records (Meyers, 1998). Bulk organic  $\delta^{13}\text{C}$  and TOC have been widely used to elucidate the source and fate of organic matter in the terrestrial, estuarine, and coastal regions (Prahl et al., 1994; Hedges et al., 1997; Zong et al., 2006, 2010b; Yu et al., 2012). TOC is a fundamental proxy that integrates the delivery to, and accumulation of, organic matter in sediments (Meyers, 1997). Normally, in continental and estuary sediments, an increase of TOC is caused by an increase in primary productivity, the supply of terrigenous organic matter, and the preservation of organic carbon (Stein, 1991). When the sedimentation rate is over 35 cm/ka, TOC content is not affected by the sedimentation rate regardless of whether the bottom conditions are anoxic or oxic (Tyson, 2001). However, in the Z09-Z core, sedimentation rates show significantly high values (with an average of 150 cm/ka). This would indicate that the preservation has little to do with the increase in TOC contents for the entire core.

As shown in Figure 6c, the 5-step running average of the TOC shows peak values for the periods 1900–1750 cal yr BP, 1500–1600 cal yr BP, 1400–1200 cal yr BP, 1000–900 cal yr BP, and 750–600 cal yr BP. This suggests an increasing organic matter input. Soils and plants are the main sources of fluvial sediment draining into the estuary (Meyers, 1997). These sediments are mixed with material from a marine source within the estuary before being deposited (Zong et al., 2006). Thus the high TOC values could be attributed to both an increase of primary marine productivity and terrestrial organic input (Zong et al., 2010b).

The materials derived from freshwater have an isotopic composition ranging from  $-23$  to  $-29\text{‰}$  (Meyers, 1997; Zong et al., 2010a, 2010b, 2010c). Meanwhile, the endogenesis marine materials have an isotopic composition ranging from  $-17$  to  $-19\text{‰}$  (Meyers, 2003). The presence of  $\text{C}_4$  land plants would complicate the interpretations of organic matter origins because their  $\delta^{13}\text{C}$  values show large differences from those of  $\text{C}_3$  plants (approximately  $-29.0 \pm 1.8\text{‰}$  and  $-13.1 \pm 0.5\text{‰}$  for  $\text{C}_3$  and  $\text{C}_4$  plants in the Pearl River Delta, respectively (Yu et al., 2010)). Jia and Peng (2003) pointed out that the dominant organic sources for modern PRE sediments are from the  $\text{C}_3$  group. Recent research by Yu et al. (2010) confirmed that the terrigenous freshwater organic matter, delivered into the estuary by river runoff, was characterized by a negative  $\delta^{13}\text{C}$  value (particle organic matters have  $\delta^{13}\text{C}$  around  $-28.7\text{‰}$ ). This indicated a dominating contribution of  $\text{C}_3$  plants. It is noteworthy that the common agricultural crop, sugarcane (a  $\text{C}_4$  plant with an average  $\delta^{13}\text{C}$  value of  $-12.7\text{‰}$ ), differs from the  $\delta^{13}\text{C}$  value for common terrestrial organic matter (Zong et al., 2010b). However, samples influenced by sugarcane input are mostly from the deltaic distributary sediments (deposited in freshwater dominated environment which has an average  $\delta^{13}\text{C}$  value around  $-23\text{‰}$  and a relatively high C/N ratio) (Zong et al., 2010b). The  $\delta^{13}\text{C}_{\text{org}}$  value of core Z09-Z ranges between  $-21.1\text{‰}$  and  $-25.3\text{‰}$ , which is similar to the isotopic composition of the shallow subtidal sediments and shallow marine sediments described by Zong et al. (2010b) but is different from typical  $\text{C}_4$  plant group. Moreover, the location of core Z09-Z lies in the shallow subtidal zone and is far away from the deltaic distributaries region, thus we assume that the influence of  $\text{C}_4$  crop in core Z09-Z is minor.

Riverine loaded materials always have higher TOC concentrations than those of the marine derived matters in the PRE (Yu et al., 2010). Therefore, the high TOC concentrations could represent an increased delivery of terrestrial organic matter. Moreover, the increased terrestrial input resulted in an increase of negative  $\delta^{13}\text{C}$  values in sediments (as terrestrial organic matters have  $\delta^{13}\text{C}$  around  $-28.7\text{‰}$  while marine-derived organic matter has  $\delta^{13}\text{C}$  around  $-21.0 \pm 0.2\text{‰}$  (Yu et al., 2010)). Thus, a lower  $\delta^{13}\text{C}$  value and a higher TOC content could reveal increased terrestrial input into the Z09-Z core (Zong et al., 2006; Yu et al., 2012). This increase would have originated from increased river runoff as illustrated by Jia and Peng (2003) and Yu et al. (2010).

The 5-step running average of  $\delta^{13}\text{C}$  distribution (Fig. 6d) in the Z09-Z core shows a good correlation with TOC (Fig. 6c). The periods 1900–1750 cal yr BP, 1650–1570 cal yr BP, 1400–1250 cal yr BP, 1000–900 cal yr BP, and 750–600 cal yr BP were marked by sharp increases in terrestrial organic input. This is indicated by the more negative  $\delta^{13}\text{C}$  values and the higher TOC content. As shown in Figures 6a and b, grain-size characteristics are consistent with the organic geochemical proxies. High sand content and MZ values exist simultaneously with the peak values of high TOC and negative  $\delta^{13}\text{C}$ . This indicates an increased river discharge into the PR and an enhanced precipitation level in the PRE area.

Since 600 cal yr BP, the variation of MZ has remained at a very stable level and the sand content has been limited. This might be due to the influences created by the increasing construction of dams and land reclamation (Li, 1991; Zong et al., 2010b). Historical literature shows that dam construction was started early during the Song Dynasty (ca. 1000 cal yr BP) in the PR. Since the start of the Ming Dynasty (ca. 600 cal yr BP), dam construction and land reclamations have undergone a process of rapid increase due to the increasing population in the PRD area (Lai, 1995). Dams inhibit the flood flushing effects in the PR and cause coarser fractions to be deposited in the dam area. This results in relative stability and a decreasing trend for the silt and sand content in the Z09-Z core (as shown in Fig. 5). The widespread land reclamations in the PRD area caused vegetation destruction. This, in turn, created increased soil erosion and therefore more terrestrial organic matters were transported into the PRE by river discharge (Zong et al., 2010b). However, both the MZ and the chemical records show high frequency oscillations in the Z09-Z core after 600 cal yr BP. Here, the relatively high TOC and lower  $\delta^{13}\text{C}$  correlated with higher MZ. This may indicate some high-frequency variations in precipitation within the PRE or just partly be due to the increased time resolution after 600 cal yr BP. Further investigation needs to be done to trace this.

#### *Climate interrelationships in the PRE*

Monsoon and tropical cyclone (typhoon) related rainfalls in the wet season (from April to September) dominate the precipitation in the PRD (Liu et al., 2001). In addition, the impact of tropical cyclones on this region is more concentrated during 7–9 months of the year. When tropical cyclones make landfall near the PRD, extreme rainfall will occur in the drainage areas (Liu et al., 2001). Therefore, the combination of tropical cyclones and monsoon rainfall brings peak precipitation to the PRD (Zhang et al., 2012). Therefore, the high river discharge events recorded in the Z09-Z core could suggest increases in summer monsoon rainfall and/or frequent typhoon landfall in the PRD and adjacent areas.

Increasing sand percentage and MZ, increasing TOC and decreasing  $\delta^{13}\text{C}$  found in sediments spanning the period 1900–1750 cal yr BP, 1650–1570 cal yr BP, 1400–1250 cal yr BP, 1100–850 cal yr BP and 750–650 cal yr BP indicate a long-term trend of strengthening precipitation-induced freshwater discharge linked to an increasing monsoon rainfall. Each of these wet events lasts for 100–300 yr. This suggests a possible centennial periodicity for the East Asian Monsoon precipitation change. Wang et al. (2005) examined the stalagmite  $\delta^{18}\text{O}$  record of Dongge Cave ( $25^{\circ}17'\text{N}$ ,  $108^{\circ}5'\text{E}$ ) from Southwest China. It is reported that the negative shifts in the stalagmite  $\delta^{18}\text{O}$  values



indicate heavy meteoric precipitation at the site (Wang et al., 2005). This, in turn, is related to changes in the amount of precipitation. Taking into account the dating uncertainties, the records from southern China appear to correlate with what retrieved from the stalagmite  $\delta^{18}\text{O}$  records (Dykoski et al., 2005) in the Dongge Cave (Fig. 7e). The stalagmite  $\delta^{18}\text{O}$  records reveal that the monsoon rainfall intensity was strengthened during periods ca. 1900 cal yr BP, 1600 cal yr BP, 1350 cal yr BP, 1150 cal yr BP, 960 cal yr BP, 720 cal yr BP and 600 cal yr BP, with a centennial period of 100–300 yr. Although the peak monsoon rainfall periods not always match well the records from core Z09-Z, considering the lower resolution of the Dongge Cave record and dating uncertainties we suggest that records from core Z09-Z and Dongge Cave vary synchronously. The similar periodicity at centennial scale, a good correlation between the multi-proxy records and stalagmite  $\delta^{18}\text{O}$  (Wang et al., 2005) both indicates that they might be driven by the same forcing mechanism, such as solar irradiation (Dykoski et al., 2005; Chen et al., 2008). Yu et al.'s (2012) recent records (core UV1, near to core Z09-Z) show a general decreasing trend in monsoonal precipitation, superimposed on apparent centennial to millennial time scales dry-wet oscillations, in the mid-Holocene. These centennial to millennial oscillations are thought to be a response to solar activity (Chen et al., 2008; Yu et al., 2012). Nevertheless, EAM rainfall records from core UV1 show minor mismatches with the Dongge Cave stalagmite  $\delta^{18}\text{O}$ . Yu et al. (2012) attributed this to the regional precipitation difference between the PRE and the Dongge Cave area.

The East Asian monsoon is a dynamic and interactive system that involves the ocean, land, and atmosphere (Peng et al., 2005). The monsoon's circulation is driven by seasonal changes in the heating contrast between the Pacific Ocean and the Asian continent. In summer, the differential heating of ocean and continent produces an atmospheric pressure gradient between the ocean and the continent. This gradient forces a steady flow of moist maritime air onto the continent and brings moisture/rainfall from the low latitudes of the Pacific Ocean to the land (Zhang and Lin, 1992). Therefore, the heat and moisture status (e.g. an El Niño phase or a La Niña phase) of the tropical western Pacific shows a close relationship with the EAM system (Mitsuguchi et al., 2008).

Figures 6a–d and f reveal that the periods of high river discharge (periods 1900–1750 cal yr BP, 1650–1570 cal yr BP, 1400–1250 cal yr BP, 1100–850 cal yr BP and 750–650 cal yr BP) basically correspond to the high intensity of the red colored unit records from Laguna Pallacocha, southern Ecuador, where it is strongly influenced by ENSO variability (Moy et al., 2002). This suggests an interrelationship between regional precipitation and ENSO events. It is well known that the inter-annual climate variation over East Asia is significantly related to the ENSO cycle (Wang et al., 2012). Recent research has shown that a negative rainfall relationship exists in northern China, while a positive rainfall relationship exists in the southern Chinese coastal areas during the summer and fall of the ENSO onset year (Tao and Zhang, 1998). This is associated with the anomalous barotropic cyclone displacing southwestward along the East Asian coast (Wu et al., 2003). ENSO mainly affects the East Asia Summer Monsoon (EASM) by modulating the locations and strength of the western North Pacific monsoon trough and the western North Pacific subtropical high (WNPSH) (Wang et al., 2009; Wu et al., 2009).

Recent research models have shown that the westward expansion of the WNPSH can increase summer precipitation in the middle and lower branches of the Yangtze River and decrease the amount of rainfall in northern China (Zeng et al., 2011). This is due to the quasi-stationary positioning of the monsoon rainfall in the 35°N region during an El Niño phase (Zhou et al., 2004). El Niño events are characterized by equatorial westerly wind anomalies near the Philippine Sea (Wang et al., 2000a). Wang and Wang's (2013) recent research has shown that this anomalous anticyclone produces southwesterly wind anomalies along the coast of southern and eastern China. These anomalies then carry moisture to southern China which increases rainfall there.

Thus, the onset of El Niño events could help to maintain summer rainfall in the middle and lower branches of the Yangtze River and in the most southern part of southern China and bring plenty of rainfall there.

Though only about 20% of total water discharge is delivered during the winter monsoon season (Zhang et al., 2012), winter precipitation may partially account for the total rainfall in the PRD. Figure 6g shows the average winter air temperature in northern China over the past 2000 cal yr BP (Wang and Wang, 1990; Zheng and Wang, 2005). High positive temperatures suggest a warmer winter and therefore a weak East Asian winter monsoon (EAWM) (Zhou and Wu, 2010). The close correspondence between the EAWM and the water discharge records suggests that the winter monsoon rainfall could have a positive effect on precipitation in the PRD. Recently, Zong et al. (2010a, 2010b, 2010c) investigated the impacts of the EAWM on the winter and rainfall in southeastern China. Their results indicate that a weak EAWM corresponds to an anomalous anti-cyclone over the South China Sea. This, in turn, induces an anomalous moisture convergence and upward motion and therefore enhances rainfall over southeastern China. Numerous studies (Zhang et al., 1999; Wang et al., 2000b; Zhang and Sumi, 2002; Wu et al., 2003; Zhou, 2010; Zhou and Wu, 2010) have shown that tropical Pacific SST anomalies (in relation to ENSO) can affect winter rainfall over Southern China. Above-normal (below-normal) winter rainfalls have been observed during El Niño (La Niña) years (Wang et al., 2000b; Wu et al., 2003) in southern China.

Furthermore, ENSO strongly affects tropical cyclone activity in the western North Pacific (Bove et al., 1998). Typhoon landfall causes large-scale disturbances to coastal aquatics. This includes such events as extreme wind velocities, storm surges, and heavy rainfall. Due to the fact that it is located in the subtropics, the southern Chinese coastal area is one of the coastlines most frequently affected by typhoons (Chan et al., 2004). Though the overall number of tropical cyclones is less affected by ENSO, the mean genesis location for typhoons generally shifts to the southeast during El Niño years (Wang and Chan, 2002). This shift results in longer lasting and more intense typhoons. The 1000-yr time series for typhoon landfalls in Southern China (Guangdong Province) indicated that the periods (1660–1680 AD, 1850–1880 AD) of most active typhoon landfalls coincided with the coldest and driest episodes recorded in central and northern China during the Little Ice Age (Liu et al., 2001). Fogarty et al. (2006b) proposed that cooler SST in the northwestern Pacific (an El Niño state), especially during the summer season, could displace the predominant storm tracks to the south. This would have made more typhoons landfall in Southern China. It has been reported that colder waters over the western north Pacific (an El Niño state) shift the subtropical high pressure farther to the west and south. This keeps tropical cyclones over lower latitudes and tracks them towards the Pearl River area (Fogarty et al., 2006a). Therefore, the onset of El Niño events could favor typhoon-derived rainfalls in the PRD. Hence, the enhanced precipitation recorded in the Z09-Z core for the past 2000 cal yr BP could be a joint result of increased monsoon rainfalls and more frequent typhoon rainfalls in the PRD.

## Conclusions

The grain-size distribution and organic geochemistry proxies of the PRE sediment can serve as reliable proxies for past changes in river discharge and regional precipitation. Increased sand fraction and higher mean grain size correspond to higher TOC and negative  $\delta^{13}\text{C}$ . These numbers reflect an increased river discharge and intensified precipitation. The multi-proxy records in the Z09-Z core offer high resolution river discharge and regional precipitation records for the past 2000 yr. Peak river discharge and precipitation occurred during the periods 1900–1750 cal yr BP, 1500–1600 cal yr BP, 1400–1200 cal yr BP, 1000–900 cal yr BP, and 750–600 cal yr BP. After 600 cal yr BP, the river discharge intensity remained at a relative stable and low level. This may reflect the increasing influence of dam constructions and land reclamations

since then. Changes in river discharge and precipitation were dominated by variations in East Asian Summer Monsoon rainfall. Typhoon related rainfall and changes in the East Asian Winter Monsoon rainfall could be positive influences on the precipitation. The frequency and intensity of ENSO would affect the regional precipitation. The onset of El Niño events could maintain summer monsoon rainfall in the most southern part of southern China. They could also enhance the winter monsoon rainfall in the PRD and adjacent area. Furthermore, El Niño events could increase typhoon-derived rainfall in the PRD.

## Acknowledgments

This project was financially supported by the National Natural Science Foundation of China (NSFC 40906038, 41230959, 41006036 and 41106043), and the Open Fund of Key Laboratory of Submarine Geosciences, SOA (MASEG201201). The authors thank Dr. Z. Yu and P. Wang for their help on the laboratory analyses for this project. Thanks also go to Dr. Y. Huang and Y. Liu for their help with sampling.

## References

- Bove, M.C., Elsner, J.B., Landsea, C.W., Niu, X.F., O'Brein, J.J., 1998. Effect of El Niño on US landfalling hurricanes, revisited. *Bulletin of the American Meteorological Society* 79, 2477–2482.
- Chan, J.C.L., Liu, K.S., Ching, S.E., Lai, E.S.T., 2004. Asymmetric distribution of convection associated with tropical cyclones making landfall along the South China Coast. *Monthly Weather Review* 132, 2410–2420.
- Chen, X., Li, Z.X., Zeng, F., Yun, Z., Xu, Z., 1993. Hydrological and water quality characteristics of the tidal river networks on the Pearl River Delta. *Proceedings of International Workshop on the Development of Strategies for Pollution Control in the Pearl River Delta*, Guangzhou, pp. 101–109.
- Chen, Z., Li, Y., Pan, J., 2004. Distributions of colored dissolved organic matter and dissolved organic carbon in the Pearl River Estuary, China. *Continental Shelf Research* 24, 1845–1856.
- Chen, F., Yu, Z., Yang, M., Ito, E., Wang, S., Madsen, D., Huang, B., Zhao, X.Y., Sato, T., John, H., Birks, B., Boomer, L., Chen, J., An, C., Wünnemann, B., 2008. Holocene moisture evolution in arid central Asia and its out-of-phase relationship with Asian monsoon history. *Quaternary Science Reviews* 27 (3–4), 351–364.
- Chen, L., Peng, S., Liu, J., Hou, Q., 2012. Dry deposition velocity of total suspended particles and meteorological influence in four locations in Guangzhou, China. *Journal of Environmental Sciences* 24, 632–639.
- Cheng, X., Qi, Y., 2007. Trends of sea level variations in the South China Sea from merged altimetry data. *Global and Planetary Change* 57, 371–382.
- Cullen, H.M., de Menocal, P.B., Hemming, S., et al., 2000. Climate change and the collapse of the Akkadian empire: evidence from the deep sea. *Geology* 28, 379–382.
- de Menocal, P.B., 2001. Cultural responses to climate change during the Late Holocene. *Science* 292, 667–673.
- Dinakaran, J., Krishnaya, N.S.R., 2011. Variations in total organic carbon and grain size distribution in ephemeral river sediments in western India. *International Journal of Sediment Research* 26, 239–246.
- Dong, L., Su, J., Ah Wong, L., Cao, Z., Chen, J.-C., 2004. Seasonal variation and dynamics of the Pearl River plume. *Continental Shelf Research* 24, 1761–1777.
- Dong, Y.X., Liu, C.L., Yin, J.R., Yang, X.Q., Franz, T.F., Gao, F.L., 2007. Late Quaternary microfaunas and paleoenvironmental changes recorded in core sediments of the Pearl River Delta, South China Sea. *Vertebrata Palasiatica* 45, 161–172.
- Dykoski, C.A., Edwards, R.L., Cheng, H., Yuan, D., Cai, Y., Zhang, M., Lin, Y., Qing, J., An, Z., Revenaugh, J., 2005. A high-resolution, absolute-dated Holocene and deglacial Asian monsoon record from Dongge Cave, China. *Earth and Planetary Science Letters* 233, 71–86.
- Fan, M., Song, C., Dettman, D.L., Fang, X., Xu, X., 2006. Intensification of the Asian winter monsoon after 7.4 Ma: grain-size evidence from the Linxia Basin, northeastern Tibetan Plateau, 13.1 Ma to 4.3 Ma. *Earth and Planetary Science Letters* 248, 186–197.
- Fogarty, E.A., Elsner, J.B., Jagger, T.H., Liu, K.B., Louie, K.S., 2006a. Variations in typhoon landfalls over China. *Advances in Atmospheric Sciences* 23, 665–677.
- Fogarty, E.A., Elsner, J.B., Jagger, T.H., Liu, K.B., Louie, K.S., 2006b. Variations in typhoon landfalls over China. *Advances in Atmospheric Sciences* 23, 665–677.
- Gao, S., Michael, C., 2001. The use of grain size trends in marine sediment dynamics: a review. *Chinese Journal of Oceanology and Limnology* 19, 265–271.
- Guo, Q., Zheng, J., Fang, X., Man, Z., Zhang, X., Zhang, P., Wang, W., 2002. Temperature changes of winter half year in Eastern China during the past 2000 years. *Quaternary Sciences* 22 (2), 166–173 (in Chinese with English abstract).
- Harrison, P.J., Yin, K., Lee, J.H.W., Gan, J., Liu, H., 2008. Physical-biological coupling in the Pearl River Estuary. *Continental Shelf Research* 28, 1405–1415.
- Hedges, J.L., Keil, R.G., Benner, R., 1997. What happens to terrestrial organic matter in the ocean? *Organic Geochemistry* 27, 195–212.
- Hollmes, J.A., Cook, E.R., Yang, B., 2009. Climate change over the past 2000 years in Western China. *Quaternary International* 194, 91–107.
- Holz, C., Stuut, J.-B.W., Henrich, R., Meggers, H., 2007. Variability in terrigenous sedimentation processes off northwest Africa and its relation to climate changes: inferences from grain-size distributions of a Holocene marine sediment record. *Sedimentary Geology* 202, 499–508.
- Huang, G., Yan, W., 1997. Foraminifera based storm surge deposition in the Holocene of the Pearl River estuary. *Chinese Science Bulletin* 42, 423–426 (in Chinese).
- Huang, Z.G., Li, P.R., Zhang, Z.Y., 1982. Formation, Development and Evolution of Zhujiang River Delta. *Guangzhou Branch of Popular Science Press*, Guangzhou 1–274 (in Chinese).
- Huang, Z.G., Zhang, W.Q., Chen, T.G., 1997. On the late Quaternary environment in Hongkong area. *Tropical Geography* 17, 157–163 (in Chinese with English abstract).
- Huang, Z., Zong, Y., Zhang, W., 2004. Coastal inundation due to sea-level rise in the Pearl River delta. *Natural Hazards* 33, 247–264.
- Huang, J., Li, A., Wan, S., 2011. Sensitive grain-size records of Holocene East Asian summer monsoon in sediments of northern South China Sea slope. *Quaternary Research* 75, 734–744.
- Iriondo, M., Brunetto, E., Kröhling, D., 2009. Historical climatic extremes as indicators for typical scenarios of Holocene climatic periods in the Pampean plain. *Palaeogeography, Palaeoclimatology, Palaeoecology* 283, 107–119.
- Jia, G.D., Peng, P.-A., 2003. Temporal and spatial variations in signatures of sedimented organic matter in Lingding Bay (Pearl estuary), southern China. *Marine Chemistry* 82, 47–54.
- Jilan, S., 2004. Overview of the South China Sea circulation and its influence on the coastal physical oceanography outside the Pearl River Estuary. *Continental Shelf Research* 24, 1745–1760.
- Jousse, H., Escarguel, G., 2006. The use of Holocene bovid fossils to infer palaeoenvironment in Africa. *Quaternary Science Reviews* 25, 763–783.
- Kuang, Y.W., Sun, F.F., Wen, D.Z., Zhou, G.Y., Zhao, P., 2008. Tree-ring growth patterns of Masson pine (*Pinus massoniana* L.) during the recent decades in the acidification Pearl River Delta of China. *Forest Ecology and Management* 255, 3534–3540.
- Lai, X., 1995. *The Chinese Local Gazettees* (in Chinese). The Commercial Press, Taipei.
- Li, S.L., 1985. Distribution of the foraminiferal thanatocoenosis of Pearl River Estuary. *Marine Geology and Quaternary Geology* 5, 83–104 (in Chinese with English abstract).
- Li, P.R., 1991. The environment evolution of the Zhujiang Delta in the last 10000 years. In: Li, P.R., Qiao, P.N., Zhen, H.H., Fang, G.Q., Huang, G.Q. (Eds.), *The Environment Evolution of the Zhujiang (Pearl River) Delta in the Last 10000 Years*. China Ocean Press, Beijing, pp. 1–79 (in Chinese).
- Li, C.C., 2004. *Formation and Evolution of Estuaries of South China*. Science Press, Beijing 1–248 (in Chinese).
- Liu, K.B., Shen, C., Louie, K.S., 2001. A 1,000-year history of typhoon landfalls in Guangdong, southern China, reconstructed with Chinese historical documentary records. *Association of American Geographers* 91, 453–464.
- Long, Y.Z., Huo, C.L., 1990. The sedimentation characteristics of Zhujiang River Delta in Late Quaternary. *Marine Science* 4, 7–13 (in Chinese with English abstract).
- Meyers, P.A., 1997. Organic geochemical proxies of paleoceanographic, paleolimnologic, and paleoclimatic processes. *Organic Geochemistry* 27, 213–250.
- Meyers, P.A., 1998. Early Holocene climatic instability in Japan: organic geochemical evidence in sediment cores from Lake Biwa, Lake Kizaki and the Japan Sea. *Journal of Asian Earth Sciences* 16, 77–83.
- Meyers, P.A., 2003. Applications of organic geochemistry to paleolimnological reconstructions: a summary of examples from the Laurentian Great Lakes. *Organic Geochemistry* 34, 261–289.
- Mitsuguchi, T., Dang, P.X., Kitagawa, H., Uchida, Shibata, T.Y., 2008. Coral Sr/Ca and Mg/Ca records in Con Dao Island off the Mekong Delta: assessment of their potential for monitoring ENSO and East Asian monsoon. *Global and Planetary Change* 63 (4), 341–352.
- Moy, C.M., Seltzer, G.O., et al., 2002. Variability of El Niño/Southern Oscillation activity at millennial time scales during the Holocene epoch. *Nature* 420, 162–165.
- Owen, R.B., 2005. Modern fine-grained sedimentation—spatial variability and environmental controls on an inner pericontinental shelf, Hong Kong. *Marine Geology* 214, 1–26.
- Peng, X.T., Zhou, H.Y., Ye, Y., Chen, G.Q., 2004. Characteristics of sediment grain size and their implications for bottom hydrodynamic environment in the Pearl River estuary. *Acta Sedimentologica Sinica* 22, 487–493 (in Chinese with English abstract).
- Peng, Y., Xiao, J., Nakamura, T., Liu, B., Inouchi, Y., 2005. Holocene East Asian monsoonal precipitation pattern revealed by grain-size distribution of core sediments of Daihai Lake in Inner Mongolia of north-central China. *Earth and Planetary Science Letters* 233, 467–479.
- Prahl, F.G., Ertel, J.R., Goni, M.A., Sparrow, M.A., Eversmeyer, B., 1994. Terrestrial organic carbon contributions to sediments on the Washington margin. *Geochimica et Cosmochimica Acta* 58, 3035–3048.
- Qiao, S., Yang, Z., Liu, J., Sun, X., Xiang, R., Shi, X., Fan, D., Saito, Y., 2011. Records of late-Holocene East Asian winter monsoon in the East China Sea: key grain-size component of quartz versus bulk sediments. *Quaternary International* 230, 106–114.
- Reimer, P.J., Baillie, M., Bard, E., Bayliss, A., Beck, J.W., Blackwell, P.G., Ramsey, C.B., Buck, C.E., Burr, George, S., Edwards, R.L., Friedrich, M., Grootes, P., Guilderson, T.P., Hajdas, I., Heaton, T.J., Hogg, A.G., Hughen, K., Kaiser, K.F., Kromer, B., McCormack, F.G., Manning, S.W., Reimer, R.W., Richards, D.A., Southon, J., 2009. Intcal09 and marine09 radiocarbon age calibration curves, 0–50,000 years cal BP. *Radiocarbon* 51, 1111–1150.
- Sasaki, N., Takahara, H., 2011. Late Holocene human impact on the vegetation around Mizorogaike Pond in northern Kyoto Basin, Japan: a comparison of pollen and charcoal records with archaeological and historical data. *Journal of Archaeological Science* 38, 1199–1208.
- Shen, C., Wang, K., Chen, B., 1989. Late Quaternary palynological assemblages in the Zhujiang (Pearl) River Delta. *Tropics Oceanology* 8, 61–69 (in Chinese with English abstract).
- Smith, D.E., Harrison, S., Firth, C.R., Jordan, J.T., 2011. The early Holocene sea level rise. *Quaternary Science Reviews* 30, 1846–1860.

- Stein, R., 1991. Accumulation of Organic Carbon in Marine Sediments. Springer, Heidelberg.
- Sun, Y., Gao, S., Li, J., 2003. Preliminary analysis of grain-size populations with environmentally sensitive terrigenous components in marginal sea setting. *Chinese Science Bulletin* 48, 184–187.
- Tanabe, S., Saito, Y., Vu, Q.L., Hanebuth, T., Ngo, Q.L., Kitamura, A., 2006. Holocene evolution of the Song Hong (Red River) delta system, northern Vietnam. *Sedimentary Geology* 187, 29–61.
- Tao, S., Zhang, Q., 1998. Response of the East Asian summer monsoon to ENSO events. *Scientia Atmospherica Sinica* 22, 399–407 (in Chinese with English abstract).
- Tyson, R.V., 2001. Sedimentation rate, dilution, preservation and total organic carbon: some results of a modeling study. *Organic Geochemistry* 32, 333–339.
- Wahl, D., Byrne, R., Schreiner, T., Hansen, R., 2006. Holocene vegetation change in the northern Peten and its implications for Maya prehistory. *Quaternary Research* 65, 380–389.
- Wang, B., Chan, J.C.L., 2002. How strong ENSO events affect tropical storm activity over the western North Pacific. *Journal of Climate* 15, 1643–1658.
- Wang, S.W., Wang, R., 1990. Variations of seasonal and annual temperatures during 1470–1979 AD in Eastern China. *Acta Meteorologica Sinica* 19, 43–59 (in Chinese with English abstract).
- Wang, C.Z., Wang, X., 2013. Classifying El Niño Modoki I and II by different impacts on rainfall in the southern China and typhoon tracks. *Journal of Climate* 26, 1322–1338.
- Wang, P.X., Bradshaw, M., Ganzei, S., Tsukawaki, S.S., Binhasan, K.W., Hantoro, S., Poobrasert, S., Burne, R., Zhao, Q.H., Kagami, H., 1997. West Pacific Marginal Seas During Last Glacial Maximum: Amplification of Environmental Signals and Its Impact on Monsoon Climate. Proceedings of 30th International Geological Congress, Utrecht, The Netherlands.
- Wang, B., Wu, R., Fu, X., 2000a. Pacific-East Asia teleconnection: how does ENSO affect East Asian climate. *Journal of Climate* 13, 1517–1536.
- Wang, B., Wu, R., Fu, X., 2000b. Pacific-East Asian teleconnection: how does ENSO affect East Asian climate? *Journal of Climate* 13, 1517–1536.
- Wang, Y., Cheng, H., Edwards, R.L., He, Y., Kong, X., An, Z.S., Wu, J., Kelly, M.J., Dykoski, C.A., Li, X., 2005. The Holocene Asian monsoon: links to solar changes and North Atlantic climate. *Science* 308, 854–857.
- Wang, F.-X., Wang, Z.-Y., Lee, J.H.W., 2007a. Acceleration of vegetation succession on eroded land by reforestation in a subtropical zone. *Ecological Engineering* 31, 232–241.
- Wang, H., Yang, Z., Saito, Y., Liu, J.P., Sun, X., Wang, Y., 2007b. Stepwise decreases of the Huanghe (Yellow River) sediment load (1950–2005): impacts of climate change and human activities. *Global and Planetary Change* 57, 331–354.
- Wang, B., Liu, J., Yang, J., 2009. Distinct principal modes of early and late summer rainfall anomalies in East Asia. *Journal of Climate* 22, 3864–3875.
- Wang, C.Z., Deser, C., Yu, J.Y., DiNezio, P., Clement, A., 2012. El Niño and Southern Oscillation (ENSO): A Review. Coral Reefs of the Eastern Pacific. Springer.
- Wong, L.A., Chen, J.C., Dong, L.X., 2004. A model of the plume front of the Pearl River Estuary, China and adjacent coastal waters in the winter dry season. *Continental Shelf Research* 24, 1779–1795.
- Wu, W., Liu, T., 2004. Possible role of the Holocene event 3 on the collapse of Neolithic cultures around the Central Plain of China. *Quaternary International* 117, 153–166.
- Wu, R.G., Hu, Z.Z., Kirtman, B.P., 2003. Evolution of ENSO-related rainfall anomalies in East Asia and the processes. *Journal of Climate* 16, 3741–3757.
- Wu, B., Zhou, T.J., Li, T., 2009. Contrast of rainfall–SST relationships in the Western North Pacific between the ENSO-developing and ENSO-decaying summers. *Journal of Climate* 22, 4398–4405.
- Xiao, S., Li, A., Liu, J.P., Chen, M., Xie, Q., Jiang, F., Li, T., Xiang, R., Chen, Z., 2006. Coherence between solar activity and the East Asian winter monsoon variability in the past 8000 years from Yangtze River-derived mud in the East China Sea. *Palaeogeography, Palaeoclimatology, Palaeoecology* 237, 293–304.
- Xu, J., 2000. Grain-size characteristics of suspended sediment in the Yellow River, China. *CATENA* 38, 243–263.
- Yao, Y., Zhan, W., Liu, Z., Zhang, Z., Zhan, M., 2008. Neotectonics of the Pearl River Delta and its relationship with the deltaic evolution. *South China Journal of Seismology* 28, 29–40.
- Yi, L., Yu, H., Ortiz, J.D., Xu, X., Qiang, X., Huang, H., Shi, X., Deng, C., 2012. A reconstruction of late Pleistocene relative sea level in the south Bohai Sea, China, based on sediment grain-size analysis. *Sedimentary Geology* 281, 88–100.
- Yu, F., Zong, Y., Lloyd, J.M., Huang, G., Leng, M., Kendrick, C., Lamb, A.L., Yim, W.-S., 2010. Bulk organic  $\delta^{13}\text{C}$  and C/N as indicators for sediment sources in the Pearl River delta and estuary, southern China. *Estuarine, Coastal and Shelf Science* 87, 618–630.
- Yu, F., Zong, Y., Lloyd, J.M., Leng, M.J., Switzer, A.D., Yim, W.W.-S., Huang, G., 2012. Mid-Holocene variability of the East Asian monsoon based on bulk organic  $\delta^{13}\text{C}$  and C/N records from the Pearl River estuary, southern China. *The Holocene* 22, 705–715.
- Zeng, X.F., Li, B., Feng, L., Liu, X.J., Zhou, T.J., 2011. East China summer rainfall during ENSO decaying years simulated by a regional climate model. *Atmospheric and Oceanic Science Letters* 4, 91–97.
- Zhang, W.Q., Huang, Z.G., 2005. A new approach to the climatic fluctuation during late Quaternary in the Pearl River Delta. *Tropical Geography* 25, 298–301 (in Chinese with English abstract).
- Zhang, J.C., Lin, Z.G., 1992. Climate of China. Wiley, New York.
- Zhang, S., Lu, X.X., 2009. Hydrological responses to precipitation variation and diverse human activities in a mountainous tributary of the lower Xijiang, China. *CATENA* 77, 130–142.
- Zhang, R., Sumi, A., 2002. Moisture circulation over East Asia during El Niño episodes in northern winter, spring and autumn. *Journal of the Meteorological Society of Japan* 80, 2213–2237.
- Zhang, R., Sumi, A., Kimoto, M., 1999. A diagnostic study of the impact of El Niño on the precipitation in China. *Advances in Atmospheric Sciences* 16, 229–241.
- Zhang, W., Wei, X., Jinhai, Z., Yuliang, Z., Zhang, Y., 2012. Estimating suspended sediment loads in the Pearl River Delta region using sediment rating curves. *Continental Shelf Research* 38, 35–46.
- Zheng, J.Y., Zheng, S.Z., 1993. An analysis on cold/warm and dry/wet in Shandong Province during historical times. *Acta Geographica Sinica* 48 (4), 348–357 (in Chinese with English abstract).
- Zheng, J., Wang, S.W., 2005. Assessment on climate change in China for the last 2000 years. *Acta Geographica Sinica* 60, 21–31.
- Zhou, L.T., 2010. Impact of East Asian winter monsoon on rainfall over southeast China and its dynamical process. *International Journal of Climatology*. <http://dx.doi.org/10.1002/joc.2101> (www.interscience.wiley.com).
- Zhou, L.T., Wu, R., 2010. Respective impacts of East Asian winter monsoon and ENSO on winter rainfall in China. *Journal of Geophysical Research* 115, D02107.
- Zhou, W., Yu, X., Jull, A.J.T., Burr, G., Xiao, J.Y., Lu, X., Xian, F., 2004. High-resolution evidence from southern China of an early Holocene optimum and a mid-Holocene dry event during the past 18,000 years. *Quaternary Research* 62, 39–48.
- Zhou, W., Long, A., Jiang, T., Chen, S., Huang, L., Huang, H., Cai, C., Yan, Y., 2011. Bacterioplankton dynamics along the gradient from highly eutrophic Pearl River Estuary to oligotrophic northern South China Sea in wet season: implication for anthropogenic inputs. *Marine Pollution Bulletin* 62, 726–733.
- Zhou, W., Yin, K., Harrison, P.J., Lee, J.H.W., 2012a. The influence of late summer typhoons and high river discharge on water quality in Hong Kong waters. *Estuarine, Coastal and Shelf Science* 111, 35–47.
- Zhou, X., Sun, L., Huang, W., Cheng, W., Jia, N., 2012b. Precipitation in the Yellow River drainage basin and East Asian monsoon strength on a decadal time scale. *Quaternary Research* 78, 486–491.
- Zong, Y., 2004. Mid-Holocene sea-level highstand along southeast coast of China. *Quaternary International* 117, 55–67.
- Zong, Y., Lloyd, J.M., Leng, M.J., Yim, W.W.-S., Huang, G., 2006. Reconstruction of Holocene monsoon history from the Pearl River estuary using diatoms and carbon isotope ratios. *The Holocene* 16 (2), 251–263.
- Zong, Y., Yim, W.W.S., Yu, F., Huang, G., 2009. Late Quaternary environmental changes in the Pearl River mouth region, China. *Quaternary International* 206, 35–45.
- Zong, Y., Kemp, A.C., Yu, F., Lloyd, J.M., Huang, G., Yim, W.W.S., 2010a. Diatoms from the Pearl River estuary, China and their suitability as water salinity indicators for coastal environments. *Marine Micropaleontology* 75, 38–49.
- Zong, Y., Yu, F., Huang, G., Lloyd, J.M., Yim, W., 2010b. Sedimentary evidence of Late Holocene human activity in the Pearl River delta, China. *Earth Surface Processes and Landforms* 35, 1095–1102.
- Zong, Y., Yu, F., Huang, G., Lloyd, J.M., Yim, W., 2010c. The history of water salinity in the Pearl River estuary, China, during the Late Quaternary. *Earth Surface Processes and Landforms* 35, 1221–1233.
- Zong, Y., Huang, K., Yu, F., Zheng, Z., Switzer, A., Huang, G., Wang, N., Tang, M., 2012. The role of sea-level rise, monsoonal discharge and the palaeo-landscape in the early Holocene evolution of the Pearl River delta, southern China. *Quaternary Science Reviews* 54, 77–88.